AIP | Applied Physics Letters

Mapping strain fields induced in Zr-based bulk metallic glasses during in-situ nanoindentation by X-ray nanodiffraction

J. Gamcová, G. Mohanty, Š. Michalik, J. Wehrs, J. Bednarčík, C. Krywka, J. M. Breguet, J. Michler, and H. Franz

Citation: Applied Physics Letters **108**, 031907 (2016); doi: 10.1063/1.4939981
View online: http://dx.doi.org/10.1063/1.4939981
View Table of Contents: http://scitation.aip.org/content/aip/journal/apl/108/3?ver=pdfcov
Published by the AIP Publishing

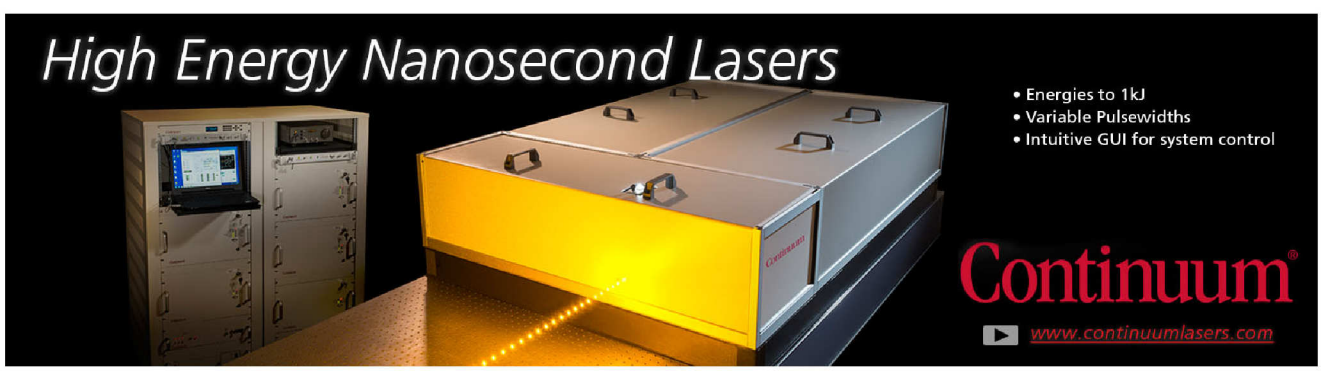

Mapping strain fields induced in Zr-based bulk metallic glasses during *in-situ* nanoindentation by X-ray nanodiffraction

J. Gamcová,[1,a)] G. Mohanty,[2] Š. Michalik,[3,b)] J. Wehrs,[2] J. Bednarčík,[1] C. Krywka,[4] J. M. Breguet,[2,5] J. Michler,[2] and H. Franz[1]
[1]*DESY, Notkestraße 85, Hamburg 22547, Germany*
[2]*Empa, Swiss Federal Laboratories for Materials Science and Technology, Laboratory for Mechanics of Materials and Nanostructures, Feuerwerkerstraße 39, Thun 3602, Switzerland*
[3]*Institute of Physics ASCR, Na Slovance 2, Praha 18221, Czech Republic*
[4]*HZG, Institut für Werkstoffforschung, Notkestraße 85, Hamburg 22547, Germany*
[5]*Alemnis GmbH, Feuerwerkerstraße 39, Thun 3602, Switzerland*

(Received 12 October 2015; accepted 5 January 2016; published online 21 January 2016)

A pioneer *in-situ* synchrotron X-ray nanodiffraction approach for characterization and visualization of strain fields induced by nanoindentation in amorphous materials is introduced. *In-situ* nanoindentation experiments were performed in transmission mode using a monochromatic and highly focused sub-micron X-ray beam on 40 μm thick Zr-based bulk metallic glass under two loading conditions. Spatially resolved X-ray diffraction scans in the deformed volume of Zr-based bulk metallic glass covering an area of $40 \times 40\ \mu m^2$ beneath the pyramidal indenter revealed two-dimensional map of elastic strains. The largest value of compressive elastic strain calculated from diffraction data at 1 N load was -0.65%. The region of high elastic compressive strains ($<-0.3\%$) is located beneath the indenter tip and has radius of 7 μm. © *2016 AIP Publishing LLC*.
[http://dx.doi.org/10.1063/1.4939981]

Despite having superior mechanical properties like high strength and hardness in comparison to crystalline materials,[1] the practical applications of bulk metallic glasses (BMGs) have been limited due to low glass formability and critical thickness. This situation changed abruptly in the nineties after the discovery of Zr-based alloys exhibiting high glass forming ability and thermal stability[2] which made these BMGs attractive for real engineering applications.[3] With a focus on structural applications, understanding the mechanical deformation behavior of BMGs has become important.[4] Among numerous experimental techniques used for objective characterization of deformation processes in BMGs, nanoindentation offers high load (micro Newton) and displacement (sub-nanometer) resolution.[5] Nanoindentation has been used to study the rate dependence of serrated flow[6] and different flow regimes in metallic glasses as a function of temperature.[7] The application of nanoindentation in combination with a technique capable of directly probing structural changes at atomic level and/or mapping strain fields with nanometer resolution will be valuable in order to reveal structure-property relationships. Transmission electron microscopy (TEM) was used for direct observation of twin deformation in thin films,[8] deformation processes in single-crystal nanoparticles,[9] and carbon nanotubes.[10] However, disadvantages of TEM include limited sample thickness and difficulties in performing strain mapping, as Keckes *et al*. have pointed out.[11] *Ex-situ* experiments on composite materials combining indentation with X-ray diffraction was earlier reported by Barabash *et al*.[12] Plastic deformation caused by indentation and visualized by X-ray computer tomography was reported by Vertyagina *et al*.[13] and Mostafavi *et al*.[14] Elastic and plastic bending experiments on BMGs were reported by Wu *et al*.[15] and Bednarcik *et al*.[16] Most of these experiments were performed during past couple of years which highlight that objective and routine techniques combining mechanical and structural properties are desired.

Using an *in-situ* technique where the material is deformed in a controlled and repeatable manner by nanoindentation and internal changes in its structure are mapped by X-ray nano- or micro-diffraction represents a non-destructive method with relatively large penetration depths of tens to hundreds of microns. X-ray diffraction (XRD) using synchrotron radiation has proven to be a suitable tool to study the local atomic structure of metallic glasses and its evolution during different types of *in-situ* experiments.[16] Yavari *et al*.[17] showed that XRD allows direct measurements of excess free volumes not only below the glass transmission temperature T_g like dilatometry but also above T_g when samples soften. Immediately after Yavari's contribution, Poulsen *et al*.[18] proposed the method for strain analysis in MGs using XRD despite the previous assumptions that X-ray scattering techniques do not allow accurate measurement of elastic strain in MGs due to inherent structural disorder. Subsequently, Hufnagel *et al*.[19] reported that the determination of elastic strain from diffraction data could be performed not only in reciprocal space but also in real space as well. Both, Poulsen and Hufnagel showed that the strain values measured by XRD in MGs are in good agreement with macroscopic observations in elastic regime.

The main objective of this work is to report the unique combination of nanoprobe tools, nanoindentation and X-ray nanodiffraction, for true *in-situ* experiments that can be used

[a)]Present address: Department of Condensed Matter Physics, Pavol Jozef Šafárik University in Košice, Park Angelinum 9, Košice, Slovakia.
[b)]Present address: Diamond Light Source Ltd., Harwell Science and Innovation Campus, Didcot, Oxfordshire OX11 0DE, United Kingdom.

to obtain a complex picture of the elastic strain distribution beneath an indenter. The strain field under the indenter in loading conditions was mapped by rastering a nano-beam and analyzing the diffraction patterns.

The combination of nanoindentation and *in-situ* nanodiffraction was demonstrated by two different experiments on two Zr-based metallic glasses. The first *in-situ* experiment was carried out on $Zr_{53}Cu_{18.7}Ni_{12}Al_{16.3}$ sample by applying constant load of 1 N. Two-dimensional map of the elastic strain field underneath the indenter tip is reported. The second *in-situ* experiment was carried out on $Zr_{50.7}Cu_{28}Ni_9Al_{12.3}$ specimen at three different loads of 0.5, 1, and 1.5 N. At each load, a vertical line scan along the loading direction was performed.

Using high purity raw materials, 5 mm thick, 5 mm wide, and 60 mm long block samples with nominal composition $Zr_{53}Cu_{18.7}Ni_{12}Al_{16.3}$ and $Zr_{50.7}Cu_{28}Ni_9Al_{12.3}$ were prepared by suction casting in a water-cooled copper mold. Slices with dimensions of 40 μm thickness and cross section of 5 mm $\times$ 5 mm were cut using a diamond cutter. *In-situ* X-ray measurements were carried out at Nanofocus Endstation of P03[20] situated at the 3rd generation synchrotron source PETRA III at DESY in Hamburg, Germany. The experimental setup is schematically described in Figure 1. An Alemnis nanoindentation platform was used for the nanoindentation measurements. Slices of samples were placed onto the sample holder (Figure 1) and aligned perpendicular to the incoming X-ray beam. A pyramidal Berkovich tip was used for the indentation experiments. A microscope mounted on the nanoindenter was used to position the sample beneath the indenter tip by utilizing a precise tip-to-optic calibration.

Spatially resolved X-ray diffraction scans were performed during indentation using a nanofocused monochromatic photon beam with an energy of 14.73 keV and size of $250 \times 300\,nm^2$ (w $\times$ h), focused by Kirkpatrick-Baez mirrors (KB mirrors). The scanning experiments were realized by translating the whole nanoindenter set-up in Y and Z directions (incoming X-ray beam in X-direction, see Figure 1) with well-defined 1.33 μm steps using a hexapod positioner. XRD patterns were collected in transmission mode by an area detector (Pilatus 1 M). The exposure time for the individual diffraction patterns was 30 s. In case of the first *in-situ* experiment on $Zr_{53}Cu_{18.7}Ni_{12}Al_{16.3}$ sample at constant load of 1 N, the size of scanned area ($40 \times 40\,\mu m^2$) was situated right beneath the sample surface that was indented (see Figure 1(a)). In case of the second *in-situ* experiment on $Zr_{50.7}Cu_{28}Ni_9Al_{12.3}$ sample, vertical line scans at three different constant loads (0.5, 1, and 1.5 N) were performed (see Figure 1(b)). The sample to detector distance was set to 190 mm in both cases, which was calibrated using a standard powder material CeO_2. Two-dimensional diffraction data were radially integrated using the program package Fit2D.[21] Such operation yielded diffracted intensity as a function of scattering vector Q ($Q = 4\pi\sin\theta/\lambda$), where θ is the half-diffraction angle and λ is the X-ray wavelength.

For an isotropic glassy material at ambient conditions, the diffraction patterns are expected to resemble perfectly circular Debye-Scherrer rings. Under applied stress, the three strain tensor components (axial, transverse, and shear-in-plane) can be obtained from the angular variation of the principal diffraction peak, as originally proposed by Poulsen *et al.*[18] As can be seen from Figure 1, only a small part of the diffraction ring was detected, which was moreover intermittent, due to the segment character of the PILATUS 1M detector. Therefore, we decided to follow peak position changes in the direction along which the force was applied. The corresponding azimuthal section used for radial integration over an angular range of 10° is shown in Figure 1 (see vertical red polygon). The profile of the principal diffraction peak was then modelled assuming a Gaussian function G(x) with a linear background. The analytical form of the applied Gaussian function was $G(x) = Aexp[-(ln2)x^2]$, where $x = (Q-Q_0)/w$, in which $2w$ is the full-width at half-maximum, Q_0 is the position of the peak maximum, and A represents the peak height. Q_0 and other profile parameters were determined by non-linear least-squares fits of the Gaussian function to a set of data points corresponding to the principal diffraction peak. Since many data points were considered for determining the peak position, the influence of the error of an individual data point on the peak position was minimized. For each integrated diffraction pattern, the shift in the position of the first diffusion maximum, Q_σ, under stress was determined with respect to the peak position Q_0 measured without stress. The relative change of the peak position upon applying an external stress σ defines the strain as $\varepsilon = (Q_0/Q_\sigma - 1)$. It should be noted here that any variations along the X-ray beam direction (sample thickness) are averaged out due to the given geometry.

Nanoindentation of the $Zr_{53}Cu_{18.7}Ni_{12}Al_{16.3}$ sample was performed in load controlled mode. In order to estimate the reference Q_0 value necessary for strain calculation, diffraction profiles were taken from the same area of the sample

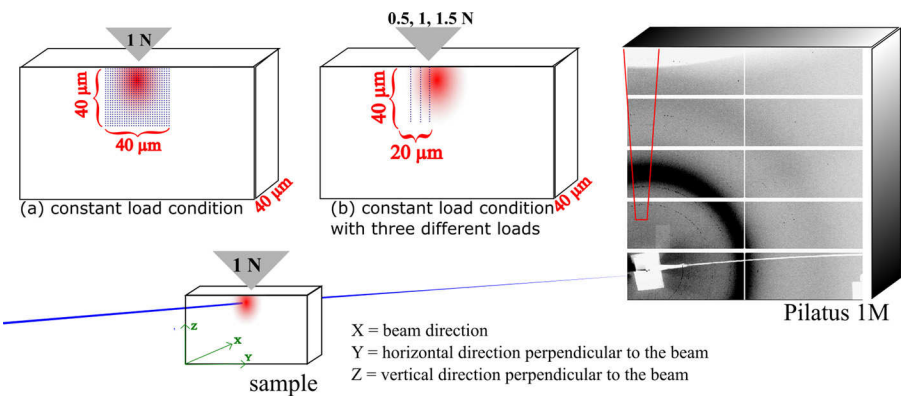

FIG. 1. Schematic view of the X-ray *in-situ* nano-diffraction experiment. In the projection on detector, a real diffraction pattern obtained during measurement is displayed (right hand side). The red polygon defines the azimuth angular section of 10° which was radially integrated. The top left part of the figure shows schematic sketch of the *in-situ* experiments: (a) performing the matrix scan on the sample while applying constant load of 1 N; (b) vertical line scans at different loads (0.5, 1, and 1.5 N).

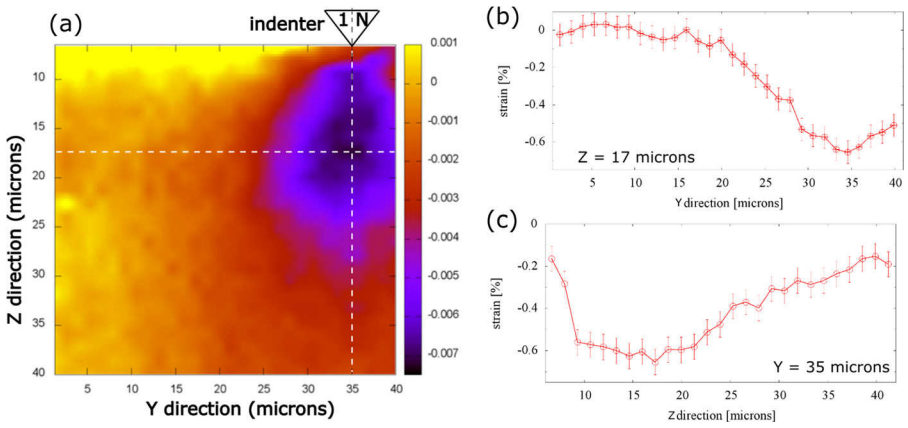

FIG. 2. (a) 2D map of strain values obtained from diffraction data from an area of 40 μm × 40 μm beneath the indenter in the load $Zr_{53}Cu_{18.7}Ni_{12}Al_{16.3}$ BMG, recorded at an applied load of 1N. White dashed lines indicate the strain profiles shown on the right hand side: (b) horizontal direction (Z = 17 μm) and (c) vertical direction (direction = 35 μm).

before applying any load. In this case, step-sizes of 10 μm and 5 μm in horizontal and vertical directions respectively, were used. Then, the Q_0 value was determined as the mean value of 32 independent measurements prior load application. Its value was $26.34 \pm 0.02\,\text{nm}^{-1}$ and within the experimental error it does not vary within the region of interest. After loading the sample to 1N, the load was held constant for more than 8.5 h during the whole *in-situ* XRD measurements. Since metallic glasses do not exhibit drastic creep effects and the indenter was placed in a temperature controlled environment, the overall change in displacement was not more than 30 nm over the duration of the test. The area beneath the Berkovich diamond tip was scanned with a step-size of 1.33 μm in Y and Z directions, in order to map in detail the structural changes induced by nanoindentation. Figure 2(a) shows a two-dimensional map of strain values obtained from the diffraction data from a 40 μm × 40 μm area beneath the position of the diamond indenter. The center of the strain field is localized at Y = 35 μm (horizontal position), Z = 17 μm (vertical position) with respect to the coordinate system used in Figure 2(a). One can easily see that the region of high elastic strains around the center of the strain field has a radius of about 7 μm. The maximum elastic strain measured for this sample and 1N load condition was −0.65% (negative sign denotes compressive stresses). There is a gradual drop in magnitude of elastic strains beneath the tip at distances greater than 20–25 μm from the center of the strain field. This behavior is demonstrated by plots in Figures 2(b) and 2(c) showing the change in strain in both vertical and horizontal directions from the center of the strain field.

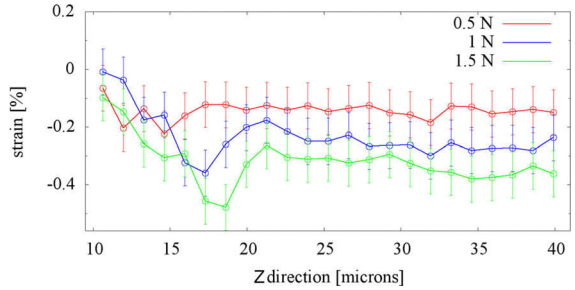

FIG. 3. Position dependence of the strains measured at three different loads of 0.5 N, 1 N, and 1.5 N, on $Zr_{50.7}Cu_{28}Ni_9Al_{12.3}$ BMG sample. The scans were taken from the same spot on the sample.

To understand the evolution of the elastic strain field with increasing load conditions, diffraction patterns were collected at three different loads (0.5, 1, and 1.5 N applied sequentially) on the $Zr_{50.7}Cu_{28}Ni_9Al_{12.3}$ sample. The idea was to explore if any changes in the strain field can be observed as a function of increasing applied load. Line scan under the indenter tip along Z direction was performed with a step-size of 1.33 μm. After every completed scan, the applied load was increased by 0.5 N at the same position without removing the indenter tip (see Figure 1(b)). The reference Q_0 value was determined from the data measured without application of the load. Its value was $26.56 \pm 0.02\,\text{nm}^{-1}$. Figure 3 shows variation of the elastic strain along the Z axis beneath the nanoindenter tip as a function of applied loads. The highest magnitudes of strain obtained from XRD data were −0.224%, −0.359%, and −0.479% for 0.5 N, 1 N, and 1.5 N, respectively.

In this study, we have introduced a novel *in-situ* approach to study the elastic deformation state of materials by combining nanoindentation and X-ray nano-diffraction. This approach was demonstrated by performing fine grid scans on the BMG sample beneath the indentation which revealed the elastic strain field in the deformation zone. The strain profile in Figure 2(a) represents experimentally observed map of elastic strains in a bulk metallic glass sample during nanoindentation obtained using real *in-situ* load-conditions experiments. It is hoped that this study will pave the way for studying strain profiles using synchrotron radiation during micromechanical testing of small volumes. In this way, the nanostructural origin of the observed strain evolution can be understood and correlated with the conditions of the deformation procedure. The setup presented in this work has become a part of the DESY sample environment group and can be used by user community performing experiments at various beamlines of the synchrotron storage ring PETRA III.

Parts of this research were carried out at the light source PETRA III at DESY, a member of the Helmholtz Association (HGF). The Nanofocus Endstation was equipped through financial support by the German Federal Ministry of Education and Research (BMBF projects 05KS7FK3 and 05K10FK3) which is also greatly acknowledged. We thank the P03 team for provision of the beam to the Nanofocus Endstation. This work has received funding from the European Community's

Seventh Framework Programme (FP7/2007-2013) under the Grant Agreement No. 312284. S.M. greatly appreciates funding from the Czech Academy of Sciences, the European Social Fund and the state budget of the Czech Republic by Grant Nos. M100101221 and CZ.1.07/2.3.00/30.0057, respectively. G.M. would like to acknowledge funding from EMPA Postdoc program cofounded by FP7: Marie Curie Actions.

[1]Q. Chen, L. Liu, and S.-M. Zhang, Front. Mater. Sci. China **4**, 34 (2010).
[2]A. Inoue, T. Zhang, N. Nishiyama, K. Ohba, and T. Masumoto, Mater. Trans., JIM **34**, 1234 (1993).
[3]M. Heilmaier, J. Mater. Process. Technol. **117**, 374 (2001).
[4]C. A. Schuh, T. C. Hufnagel, and U. Ramamurty, Acta Mater. **55**, 4067 (2007).
[5]C. Schuh and T. Nieh, J. Mater. Res. **19**, 46 (2004).
[6]C. Schuh, T. Nieh, and Y. Kawamura, J. Mater. Res. **17**, 1651 (2002).
[7]C. A. Schuh, A. C. Lund, and T. Nieh, Acta Mater. **52**, 5879 (2004).
[8]J. H. Lee, X. Zhang, and H. Wang, J. Appl. Phys. **109**, 083510 (2011).
[9]C. Carlton and P. Ferreira, Micron **43**, 1134 (2012).
[10]P.-C. Tsai, Y.-R. Jeng, Y.-X. Huang, and K.-T. Wu, Appl. Phys. Lett. **103**, 053119 (2013).
[11]J. Keckes, M. Bartosik, R. Daniel, C. Mitterer, G. Maier, W. Ecker, J. Vila-Comamala, C. David, S. Schoeder, and M. Burghammer, Scr. Mater. **67**, 748 (2012).
[12]R. I. Barabash, H. Bei, Y. F. Gao, and G. E. Ice, Acta Mater. **58**, 6784 (2010).
[13]Y. Vertyagina, M. Mostafavi, C. Reinhard, R. Atwood, and J. Marrow, J. Eur. Ceram. Soc. **34**, 3127 (2014).
[14]M. Mostafi, D. M. Collins, B. Cai, R. Bradley, R. C. Atwood, C. Reinhard, X. Jiang, M. Galano, P. D. Lee, and T. J. Marrow, Acta Mater. **82**, 468 (2014).
[15]Y. Wu, A. D. Stoica, Y. Ren, D. Ma, Y. F. Gao, and H. Bei, Intermetallics **67**, 132 (2015).
[16]J. Bednarcik, L. Chen, X. Wang, J. Jiang, and H. Franz, Metall. Mater. Trans. A **43**, 1558 (2012).
[17]A. R. Yavari, A. Le Moulec, A. Inoue, N. Nishiyama, N. Lupu, E. Matsubara, W. J. Botta, G. Vaughan, M. Di Michiel, and Å. Kvick, Acta Mater. **53**, 1611 (2005).
[18]H. F. Poulsen, J. A. Wert, J. Neuefeind, V. Honkimäki, and M. Daymond, Nat. Mater. **4**, 33 (2005).
[19]T. Hufnagel, R. Ott, and J. Almer, Phys. Rev. B **73**, 064204 (2006).
[20]C. Krywka, J. Keckes, S. Storm, A. Buffet, S. V. Roth, R. Döhrmann, and M. Müller, J. Phys. Conf. Ser. **425**, 072021 (2013).
[21]A. P. Hammersley, S. O. Svensson, M. Hanfland, A. N. Fitch, and D. Hausermann, High Pressure Res. **14**, 235–248 (1996).